

Article

**Hydration and Reduction of Molecular Beam Epitaxy
Grown VO₂-FeO(0001): Ambient Pressure Study**

Chang-Yong Kim, Jeffrey A. Klug, Peter C. Stair, and Michael J. Bedzyk

J. Phys. Chem. C, **2009**, 113 (4), 1406-1410 • Publication Date (Web): 05 January 2009

Downloaded from <http://pubs.acs.org> on January 27, 2009

More About This Article

Additional resources and features associated with this article are available within the HTML version:

- Supporting Information
- Access to high resolution figures
- Links to articles and content related to this article
- Copyright permission to reproduce figures and/or text from this article

[View the Full Text HTML](#)



ACS Publications
High quality. High impact.

Hydration and Reduction of Molecular Beam Epitaxy Grown VO_x/α-Fe₂O₃(0001): Ambient Pressure Study

Chang-Yong Kim,^{*,†} Jeffrey A. Klug,[‡] Peter C. Stair,[§] and Michael J. Bedzyk[†]

Department of Materials Science and Engineering, Department of Physics and Astronomy, and Department of Chemistry, Northwestern University, Evanston, Illinois 60208

Received: May 10, 2008; Revised Manuscript Received: September 29, 2008

Supported vanadium oxides processed under ambient environments have been studied by using X-ray standing wave (XSW) analysis of X-ray fluorescence spectroscopy and X-ray photoelectron spectroscopy (XPS). For the VO_x/α-Fe₂O₃(0001) system, hydration and hydrogen annealing have been carried out under ambient pressure. Vanadium in the hydrated oxide phase occupies two high-symmetry surface adsorption sites with distinct adsorption heights, which resembles the adsorption geometry of fully oxidized vanadium. Reduction by the hydrogen annealing enhanced the V overlayer ordering by relocating a portion of the disordered V to high-symmetry sites. The V atoms located closer to the substrate oxygen layer in the hydrated phase moved toward the substrate after hydrogen reduction, while the V in the higher adsorption site stayed at the same height. The different responses of two adsorption sites to the reduction process are discussed and related to activities of the two sites.

Introduction

Hydration and activation of supported catalysts are common processes encountered during the life cycle of a catalyst. The hydrated phase is the typical form of catalysts prepared by a wet chemical impregnation. For catalysts prepared by other methods, hydration can occur through exposure to the air. Occasionally, the H₂O evolves as an active ingredient or byproduct of a catalytic reaction,¹ and water partial pressure or degree of hydration can affect catalytic activities.^{2,3}

It has been known that the hydration of catalysts can perturb the adsorption geometry of catalysts by breaking bonds between catalyst cations and the supporting substrate and subsequently by forming hydroxyl groups at the broken ends.^{4–6} However, little or no hydration-induced structural disturbance has been observed for a number of substrate systems, including α-Fe₂O₃(0001).^{7–11}

Activation of the (hydrated) catalysts usually involves high-temperature annealing in the presence of a reducing agent.¹² The most common reducing agents are hydrogen and carbon monoxide gas. Numerous experiments have been conducted to study the atomic-scale structure of catalysts in the hydrated, dehydrated, and activated phases.^{5,13–19} Some of these studies use single crystal substrates and apply numerous ultrahigh vacuum (UHV) surface characterization tools. However, it is oftentimes questionable to extend experimental conclusions deduced from UHV measurements to ambient pressure reaction conditions. This so-called “pressure gap problem” is still under intense debate. In the present study, we compare the reduction process under an ambient H₂ environment with our previously reported atomic-hydrogen reduction in UHV.²⁰

In our previous study, we used X-ray photoemission spectroscopy (XPS) and the X-ray standing wave (XSW) imaging

method to study the redox-induced reversible adsorption geometry change of the vanadium cations supported on a single crystal α-Fe₂O₃(0001) surface.²⁰ This previous UHV redox study had 0.5 monolayer (ML) of vanadium deposited at room temperature by molecular beam epitaxy (MBE) followed by in situ room temperature exposure to atomic oxygen and then atomic hydrogen beams. Herein, we extend this previous UHV study to an ambient environment by using a second MBE prepared 0.5 ML VO_x/α-Fe₂O₃(0001) sample. The electronic and atomic scale structural changes induced by ambient hydration and subsequent reduction are studied.

Experimental Methods

The α-Fe₂O₃ has corundum structure with lattice parameters of $a \equiv b = 5.038 \text{ \AA}$, $c \equiv 13.772 \text{ \AA}$, $\alpha \equiv \beta = 90^\circ$, $\gamma \equiv 120^\circ$.²¹ The $10 \times 10 \times 1 \text{ mm}^3$ α-Fe₂O₃ (0001) single crystal surfaces were cleaned in UHV by annealing at 450 °C in an atomic oxygen beam. The atomic oxygen was produced by passing the molecular oxygen through a hot refractory metal tube at 975 °C. Vanadium was deposited onto a clean room temperature α-Fe₂O₃(0001) surface from a K-cell evaporation source of vanadium metal held at 1547 °C. During vanadium deposition, the pressure was typically 2×10^{-9} Torr.

To produce a hydrated phase, the as-deposited samples were taken out from UHV and briefly exposed to the air. For XPS measurements, the hydrated sample was reintroduced to UHV through a sample load-lock chamber. The load-lock chamber was equipped with a halogen lamp that was used to heat the sample under 15 Torr of H₂ during reduction of the vanadium oxide. For the XSW measurements, the sample was installed inside a Be-dome minichamber and was kept in a high vacuum during the measurements. Inside the Be-dome, the sample was mounted on a heater with a graphite filament embedded in pyrolytic boron nitride (GE ceramics), and the reduction process was carried out by annealing the sample at 450 °C under a continuous flow of 2% hydrogen balanced with 98% He gas. Prior to the reduction treatments, the hydrated samples were

* Corresponding author. Current address: Canadian Light Source Inc., 101 Perimeter Road, Saskatoon, SK S7N 0X4, Canada. E-mail: Chang-Yong.Kim@lightsources.ca.

[†] Department of Materials Science and Engineering.

[‡] Department of Physics and Astronomy.

[§] Department of Chemistry.

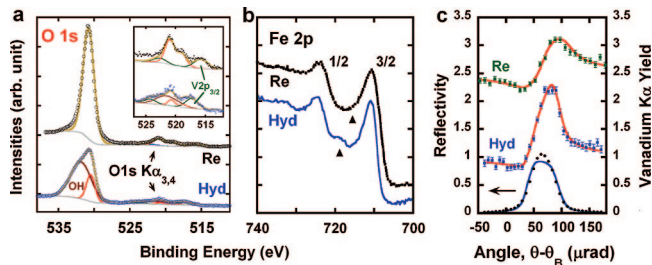


Figure 1. X-ray photoelectron spectra of (a) O 1s, V 2p, and (b) Fe 2p taken with an electron takeoff angle of 25° from the sample surface. (a and b) The XPS spectra are displaced vertically for clarity with hydrated phase (Hyd) at the bottom and reduced phase (Re) at the top. (a) Details of V 2p spectra are shown in the inset. The O and V spectra were fit with O 1s, (OH)⁻ 1s, and V 2p_{1/2} and 2p_{3/2} doublet, which are represented by solid lines. (b) Arrows between the Fe 2p_{1/2} and 2p_{3/2} peaks mark satellite peaks originating from Fe²⁺ (Re) or Fe³⁺ (Hyd). (c) XSW data and analysis for the (10 $\bar{1}$ 4) Bragg reflection showing the reflectivity (bottom) and vanadium K α fluorescence modulations of Hyd and Re.

heated at 180 °C under 1 atm of oxygen for the XPS or under flowing oxygen gas environment for the XSW measurements.

The XPS measurements were conducted in an UHV chamber with a base pressures of 5×10^{-11} Torr by using Al K α radiation (without a monochromator) and a hemispherical analyzer for photoelectron energy analysis. The XSW measurements were conducted at the Advanced Photon Source (APS) 5ID-C beamline²² at an incident energy of 7.00 keV and used an X-ray fluorescence (XRF) solid-state detector to monitor the V K α XRF yield. The vanadium surface coverage was controlled by deposition time and was determined as 0.5 ML by comparing the XRF yield from the sample with standard sample calibrated with Rutherford backscattering spectroscopy. The coverage of 1 ML is defined as the area density of Fe ions in the (0001) surface, 9.1 atoms /nm². For XSW analysis, the XRF yield of a selected atomic species is measured while scanning in angle through an hkl substrate Bragg reflection.^{23–26} The amplitude (f_H) and phase (P_H) of the $H = hkl$ Fourier component of the fluorescent atom density distribution can be measured directly from the modulation of the XRF yield. As recently demonstrated, a summation of these XSW measured Fourier components generates an element-specific real-space 3D atom distribution map.^{22,25,27–30}

Results

From our XPS data shown in Figure 1a, the vanadium in a hydrated phase has its 2p_{3/2} photoelectron binding energy (BE) at 517.45 eV, corresponding to a 5+ oxidation state. In the binding energy range of O 1s and V 2p core levels the measured spectra consisted of photoelectrons from substrate oxygen,

surface hydroxyl group (OH⁻), and vanadium oxide. To determine the oxidation state of the vanadium, line shape analysis was performed through nonlinear least-squares curve fit of measured spectra to the sum of individual PE lines which were represented by the Voigt functional form (Lorentzian function convoluted with Gaussian function) with Shirley background contribution. The fit spectra consist of the vanadium 2p_{3/2} and 2p_{1/2} doublet and O 1s contributed from the substrate oxygen and adsorbed OH⁻. Because an Al X-ray source was used without a monochromator, the incident X-ray beam has Al K $\alpha_{3,4}$ in addition to the major K $\alpha_{1,2}$ radiation. Through the fit the ratio between photoelectron intensities excited by Al K $\alpha_{1,2}$ and K $\alpha_{3,4}$ are fixed to the intensity ratio of O 1s excited by K $\alpha_{1,2}$ and K $\alpha_{3,4}$ measured from the clean α -Fe₂O₃(0001) substrate. Reported values for various vanadium oxides are V³⁺ at 515.3–515.85 eV, V⁴⁺ at 515.8–516.2, and V⁵⁺ at 516.9–517.2 eV.^{31–33} Hydrogen annealing reduced the vanadium cations to 3+ (V 2p_{3/2} BE of 515.3 eV). The BE difference between O 1s and V 2p_{3/2} has been used to determine the oxidation state of vanadium, and reported values are 12.8, 14.16, and 14.71 eV for V⁵⁺, V⁴⁺, and V³⁺ respectively.³² The BE differences in the present study are 13.0 and 15.0 eV for the hydrated and reduced phases, respectively. Hence the V oxidation state of the hydrogen annealed phase can be assigned to 3+ confidently. For VO_x/Al₂O₃ the average oxidation state of +3.5 has been reported after H₂ annealing at similar temperature.³⁴ It is worth noting that for our earlier reported UHV prepared surfaces the binding energies of V 2p_{3/2} in the oxidized and reduced phases were 516.9 and 515.3 eV, respectively.²⁰ In the hydrated surface the oxygen 1s spectrum has a shoulder at 1.3 eV higher on the BE side of the main peak, which can be attributed to an OH group.^{35,36} The oxidation state change of the interface Fe can be seen in the Fe 2p XPS in Figure 1b, where increased contribution from Fe²⁺ changes the spectrum profile similar to the UHV study.²⁰ By accepting electrons donated by the vanadium, a fraction of the Fe ions in the 3+ oxidation state are reduced to the 2+ oxidation state, concurrently with reduction of the vanadium from the hydrated phase (5+) to reduced phase (3+).

The hydrated and reduced surfaces show distinct V adsorption geometry, as seen from the (10 $\bar{1}$ 4) XSW measurements (Figure 1c). Table 1 summarizes the XSW analysis results from the hydrated and reduced V/ α -Fe₂O₃(0001) surfaces. The recently developed XSW imaging method^{20,27,29,30,37} based on the Fourier inversion of XSW measured f_H and P_H values has been applied. Figure 2 shows 2D cuts through the reduced and oxidized 3D V atomic density maps, which make it possible to identify adsorption sites and their relative occupancies in a model-independent way. Due to the nature of the Fourier transform, the XRF-selected 3D atomic density map has a periodicity imposed by the primitive unit cell of the substrate, which for

TABLE 1: Summary of the XSW Measurement (meas) Results from the Hydrated and Reduced Surface Treatments of the 0.5 ML V/ α -Fe₂O₃(0001) Surface^a

(hkl)	$d_{hkl}(\text{Å})$	hydrated				reduced			
		f_H^{meas}	f_H^{calc}	P_H^{meas}	P_H^{calc}	f_H^{meas}	f_H^{calc}	P_H^{meas}	P_H^{calc}
(0006)	2.30	0.43(2)	0.55	0.93(1)	0.93	0.47(3)	0.51	0.91(1)	0.86
(10 $\bar{1}$ 4)	2.70	0.42(2)	0.44	0.52(1)	0.50	0.69(1)	0.73	0.40(1)	0.40
(01 $\bar{1}$ 2)	3.69	0.29(1)	0.27	0.40(1)	0.39	0.21(2)	0.18	0.45(2)	0.46
(02 $\bar{2}$ 4)	1.84	0.47(2)	0.44	0.47(1)	0.50	0.77(2)	0.73	0.38(1)	0.40
(11 $\bar{2}$ 6)	1.70	0.56(1)	0.55	0.93(1)	0.93	–	–	–	–

^a The measured f_H and P_H values for V from different $H = (hkl)$ Bragg reflections are compared to those calculated from the best-fit models described in Table 2. Related to the notation of experimental errors, 0.43(2) represents 0.43 ± 0.02 .

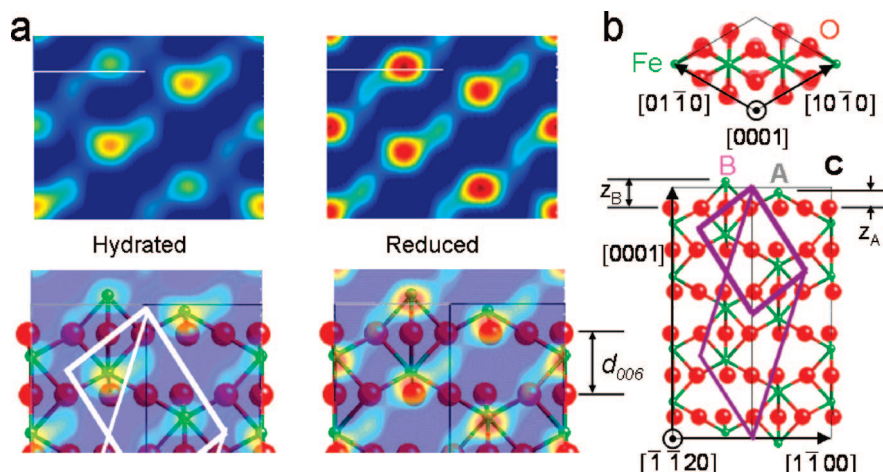


Figure 2. (a) The $(\bar{1}\bar{1}20)$ 2D cuts through the XSW measured 3D vanadium atomic density maps for the hydrated and reduced $V/\alpha\text{-Fe}_2\text{O}_3(0001)$ surface. As a reference, the $(\bar{1}\bar{1}20)$ projection of the $\alpha\text{-Fe}_2\text{O}_3$ structure is overlapped with the 2D cuts in the bottom. (b) Projections of the $\alpha\text{-Fe}_2\text{O}_3$ ball and stick model. The high-symmetry sites A–C are indicated. The z_A and z_B indicate adsorption heights used in model fit. (a,b) Two parallelograms represent intersections of the “effective” and the primitive unit cells with the $(\bar{1}\bar{1}20)$ plane.

TABLE 2: Best Fit Parameters for V Adsorption Geometry Model

surface	c_A	c_B	$z_A(\text{\AA})$	$z_B(\text{\AA})$
hydrated	0.38(2)	0.22(2)	0.29(2)	0.60(3)
reduced	0.40(2)	0.41(2)	0.09(4)	0.57(4)

$\alpha\text{-Fe}_2\text{O}_3$ is rhombohedral. However, for any given (0001) surface structure, six chemically equivalent surfaces separated by the interlayer distance between oxygen layers (d_{0006}) would exist with equal probability.³⁸ Hence, atoms adsorbed on these six surfaces would see the same local environment. As a result of the six surface terminations, the “effective” primitive unit cell (3D periodicity) for the V density map is half of the rhombohedral cell. Figure 2 shows the intersections of the “effective” and primitive unit cells with the $(\bar{1}\bar{1}20)$ cut plane.

For the $\alpha\text{-Fe}_2\text{O}_3(0001)$ surface, there are two high-symmetry Fe sites (A and B) above the topmost oxygen layer that are symmetrically equivalent to the Fe occupied octahedral sites in the bulk. The A-site is located closer to the underlying oxygen layer than the B-site. The high-symmetry V adsorption sites, which are compatible with the images, are labeled as A and B in Figure 2. The maps clearly show the A- and B-sites as adsorption sites in the hydrated and reduced surfaces.

In order to quantify the occupation fractions and heights for sites A and B, we performed a least-squares fit of a model to the measured f_H and P_H sets for each surface. The model has four parameters: c_A and c_B representing the fractions of V atoms occupying site-A and -B and z_A and z_B are the respective adsorption heights of V atoms above the unrelaxed oxygen plane (See Figure 2). On the basis of this model, the H th Fourier component for the V atomic distribution is

$$\begin{aligned}
 F_H &= f_H \exp(2\pi i P_H) \\
 &= \sum_j c_j \exp(2\pi i H \cdot r_j) \\
 &= c_A \exp\left(2\pi i \frac{2h+k}{3}\right) \exp(2\pi i l z_A) + \\
 &\quad c_B \exp\left(2\pi i \frac{h+2k}{3}\right) \exp(2\pi i l z_B) \quad (1)
 \end{aligned}$$

Inclusion of the Debye–Waller (DW) factor does not improve the fit, which might indicate that the experimental error is bigger than DW corrections. Also it should be pointed out that actual

surfaces might have more complex adsorption geometry than the model describes, as can be seen by the rather large discrepancy in the best fit value of P_{0006} in the reduced phase (Table 1). In a separate model procedure, lateral offsets from high symmetry sites were included but converged to zero within an error of 0.07 \AA .

The parameters from the best fits, which are listed in the Table 2, quantitatively demonstrate that reduction of the vanadium causes the V atoms in the A-sites to shift down closer to the underlying oxygen layer and partially redistribute randomly distributed V atoms to B-sites.³⁹ The concurrent reduction to V^{3+} and Fe^{2+} caused V atoms to accumulate in B-sites, while the XSW measured adsorption height does not change significantly. The bond lengths between the V and the underlying oxygen are in the range of 1.64–1.78 if the topmost oxygen layer is in an unperturbed bulk position. These bond lengths are small compared to typical V–O bond lengths of 1.97 and 2.05 \AA for corundum V_2O_3 .⁴⁰ As pointed out by theoretical calculations, the small bond lengths can be explained by the reduced number of coordinate oxygens and the increased interaction between the adsorbed V and the bulk Fe ions under the top oxygen layer.^{41,42}

Discussions

From our previous UHV study²⁰ the as-deposited VO_x phase has been characterized by V^{3+} adsorbed in A- and C-sites. After exposure of the as-deposited phase to the atomic oxygen, the V atoms change to 5+ oxidation state and occupy A- and B-sites. Subsequent exposure of the oxidized phase to the atomic hydrogen moved the V back to A- and C-sites and changed the oxidation state to 3+. The as-deposited and reduced phases are essentially the same phase and the UHV redox processes with atomic oxygen and hydrogen exposures induce reversible changes of oxidation states and adsorption geometries.

In the present study, the hydrated phase has been prepared by the air exposure of the UHV as-deposited (reduced) phase. The hydration changed the oxidation state of V from 3+ to 5+. The XSW analysis indicates that the hydration alters not only the oxidation state but also the adsorption geometry, which involves adsorption site switchover from C- to B-site. That is, in the hydrated phase, V occupies A- and B- sites similar to the UHV prepared oxidized phase. Average adsorption heights of the V in hydrated phase, with respect to the bulk lattice plane,

were decreased compared to the UHV prepared oxidized phase. It is worth noting that XSW measured heights of adsorbed V are referenced to the unrelaxed bulk layer position. If there is a hydration induced relaxation in top layers of α -Fe₂O₃(0001) substrate, V height measured from the bulk reference layer changes by the relaxation, even if the distance between V and the top surface layer does not change. Also breaking of the V–O–substrate bond by hydration could result in a decreased adsorption height of V atoms. From the current study, the origin of the overall decrease in the V adsorption height is unclear.

Although they have the same oxidation state, the adsorption geometry of the V in the reduced phase prepared by 2% hydrogen annealing of the hydrated phase differs from geometry of the UHV-prepared reduced phase. In the UHV reduced phase, V occupies A- and C-sites instead of A- and B-sites, which are observed from the 2% H₂ reduction. These different adsorption geometries and the overall height of V cation after ambient reduction process can be related to (1) the existence of hydroxyl groups on the surface and (2) the reduction method involving molecular hydrogen annealing in the current study. During the UHV reduction by atomic hydrogen exposure, the sample was kept at room temperature to minimize a thermal effect in reversible redox processes studies. In the current study, there was annealing of the sample at 180 °C in an O₂ environment and at 450 °C under 2% hydrogen flow. The V atoms adsorbed on the C- site may be metastable and could migrate irreversibly to A- and B- sites during the annealing. Adsorption geometry of the V in the 180 °C annealed dehydrated phase was not investigated, and it is unclear whether the irreversible change has been induced by a dehydration or reduction process. Theoretical calculations indicated that the C-site is not an energetically stable adsorption site, and also simultaneous occupation of the A- and C-sites is less stable compared to occupation of A- and B-sites.⁴¹

As a result of the ambient reduction, the A-site vanadium moved considerably lower, while the adsorption height of the V in the B-site remained constant within experimental error. A similar change of bond length induced by oxidation state change of adsorbed cation has been observed in various systems. It has been known that supported cations make bonds with additional oxygen or hydroxyl groups, and subsequently, the bonding between substrate and cations becomes weak by partial transfer of bonding electrons between substrate and cations to the new bond.^{43,44} As a result of the weakened bond, the adsorption height of the cation from the substrate increases. The adsorption height could decrease when the reduction removes the extra bonding between cations and the oxygen or OH. This explanation indicates that the A-site, which is closer to the underlying oxygen layer, is more sensitive to a subtle electron redistribution. For certain redox processes, the lattice oxygen bonds with a reactive chemical species and leaves the surface. The removed lattice oxygen from the substrate is refilled quickly by the extra oxygen bonded to the cations. Such a perturbation and a mild sample annealing during the reduction process might be responsible for the adsorption height changes.

Often acid–base property has been used to characterize active sites and predict chemical reactions taking place at the sites.^{45–47} Experimental works from Fe₂O₃ powder has shown that Fe₂O₃ can be classified as an acido–basic oxide⁴⁸ with Brønsted and Lewis acid sites⁴⁹ and Brønsted basicity.⁵⁰ Experimental works from single crystalline α -Fe₂O₃(0001) film have found the acidic character of the Fe atoms underneath the topmost oxygen layer along with basic O sites.⁵¹ As theoretical calculations indicated, there is increased interaction between the

V in A- and B-sites with the second layer Fe atoms and it can be postulated that the A- and B-sites can act as acidic sites. The C-site does not have the second layer Fe and the C-site can be more basic due to the O atoms underneath. However, characterization of acid–base properties of the sites requires more studies. For example, the XSW analysis of photoelectron spectra of probing molecules²⁶ can provide details of dissociation and site-specific acid-basic properties.

The H₂ reduction increased the occupation of V in the B-site. This enhanced coherent adsorption of the V was observed also in UHV reduction. It is also worth noting that the total O 1s intensity, including OH shoulder, changes little after H₂ reduction. The hydroxyl group might be generated initially by dissociative adsorption of water molecule around defect sites. After the hydrogen annealing process, a large portion of the oxygen in hydroxyl groups converts to lattice oxygen to cure defect sites rather than desorbing from the surface as H₂O. This improved ordering of the substrate could partially explain the enhanced ordering of the V after reduction.

In summary, ambient pressure hydration and reduction of a supported vanadium oxide on α -Fe₂O₃(0001) has been studied by XPS and XSW measurements. The V had a 5+ oxidation state in the hydrated phase and reduction by hydrogen annealing changed the oxidation state to 3+. The ordered portion of vanadium occupies two high symmetry sites with distinct adsorption heights for both hydrated and reduced phases. The reduction process enhanced the V overlayer ordering by relocating a portion of disordered V that existed in the hydrated phase to high symmetry sites with a higher adsorption site height. The adsorption geometry of the V in the higher adsorption site was intact after the reduction process, in contrast to a big shift down of the V in lower adsorption site. The different responses to reduction from the two adsorption sites might be related to the different reactivity of the sites. Further studies with various reaction gases other than the hydrogen are required to address site-specific chemical reactivity.

Acknowledgment. The authors thank the DND-CAT staff for technical assistance. This work was supported by the DOE under contract No. DE-FG02-03ER15457 to the Institute for Catalysis in Energy Processes (ICEP) at Northwestern University (NU). Use of the APS at Argonne National Laboratory was supported by the DOE/BES under Contract No. DE-AC02-06CH11357. DND-CAT is supported in part by the State of Illinois. This work made use of NU Central Facilities supported by the MRSEC through NSF Contract No. DMR-0520513.

References and Notes

- (1) Hu, H. C.; Wachs, I. E. *J. Phys. Chem.* **1995**, *99*, 10911.
- (2) Mamedov, E. A.; Corberan, V. C. *Appl. Catal., A* **1995**, *127*, 1.
- (3) Jehng, J. M.; Deo, G.; Weckhuysen, B. M.; Wachs, I. E. *J. Mol. Catal. A: Chem.* **1996**, *110*, 41.
- (4) Chan, S. S.; Wachs, I. E.; Murrell, L. L.; Wang, L.; Hall, W. K. *J. Phys. Chem.* **1984**, *88*, 5831.
- (5) Deo, G.; Wachs, I. E. *J. Phys. Chem.* **1991**, *95*, 5889.
- (6) Wachs, I. E. *Catal. Today* **1996**, *27*, 437.
- (7) Kurtz, R. L.; Henrich, V. E. *Phys. Rev. B* **1982**, *26*, 6682.
- (8) Kurtz, R. L.; Henrich, V. E. *Phys. Rev. B* **1983**, *28*, 6699.
- (9) Kurtz, R. L.; Henrich, V. E. *J. Vac. Sci. Technol., A* **1984**, *2*, 842.
- (10) Kurtz, R. L.; Henrich, V. E. *Phys. Rev. B* **1987**, *36*, 3413.
- (11) Liu, P.; Kendelewicz, T.; Brown, G. E.; Nelson, E. J.; Chambers, S. A. *Surf. Sci.* **1998**, *417*, 53.
- (12) Wachs, I. E.; Weckhuysen, B. M. *Appl. Catal., A* **1997**, *157*, 67.
- (13) Rupprechter, G.; nther; Weilach, C. *J. Phys.: Condens. Matter* **2008**, *20*, 184019.
- (14) Akita, T.; Okumura, M.; Tanaka, K.; Tsubota, S. *J. Electron Microsc.* **2004**, *53*, 29.
- (15) Maurice, V.; Cadot, S.; Marcus, P. *Surf. Sci.* **2000**, *458*, 195.

- (16) Lianos, L.; Debauge, Y.; Massardier, J.; Jugnet, Y.; Bertolini, J. C. *Catal. Lett.* **1997**, *44*, 211.
- (17) Somorjai, G. A. *Catal. Lett.* **1992**, *15*, 25.
- (18) Kim, K. S.; Barteau, M. A. *J. Catal.* **1990**, *125*, 353.
- (19) Henderson, M. A. *Surf. Sci. Rep.* **2002**, *46*, 1.
- (20) Kim, C.-Y.; Escudero, A. A.; Stair, P. C.; Bedzyk, M. J. *J. Phys. Chem. C* **2007**, *111*, 1874.
- (21) Blake, R. L.; Hessevic, Re; Zoltai, T.; Finger, L. W. *Am. Mineral.* **1966**, *51*, 123.
- (22) Walko, D. A.; Sakata, O.; Lyman, P. F.; Lee, T.-L.; Tinkham, B. P.; Okasinski, J. S.; Zhang, Z.; Bedzyk, M. J. *AIP Conf. Proc.* **2004**, *705*, 1166.
- (23) Golovchenko, J. A.; Patel, J. R.; Kaplan, D. R.; Cowan, P. L.; Bedzyk, M. J. *Phys. Rev. Lett.* **1982**, *49*, 560.
- (24) Zegenhagen, J. *Surf. Sci. Rep.* **1993**, *18*, 199.
- (25) Bedzyk, M. J.; Cheng, L. W. *Rev. Mineral. Geochem.* **2002**, *49*, 221.
- (26) Woodruff, D. P. *Rep. Prog. Phys.* **2005**, *68*, 743.
- (27) Cheng, L.; Fenter, P.; Bedzyk, M. J.; Sturchio, N. C. *Phys. Rev. Lett.* **2003**, *90*, 255503.
- (28) Escudero, A. A.; Goodner, D. M.; Okasinski, J. S.; Bedzyk, M. J. *Phys. Rev. B* **2004**, *70*, 235416.
- (29) Zhang, Z.; Fenter, P.; Cheng, L.; Sturchio, N. C.; Bedzyk, M. J.; Machesky, M. L.; Wesolowski, D. J. *Surf. Sci.* **2004**, *554*, L95.
- (30) Kim, C.-Y.; Elam, J. W.; Pellin, M. J.; Goswami, D. K.; Christensen, S. T.; Hersam, M. C.; Stair, P. C.; Bedzyk, M. J. *J. Phys. Chem. B* **2006**, *110*, 12616.
- (31) Sawatzky, G. A.; Post, D. *Phys. Rev. B* **1979**, *20*, 1546.
- (32) Silversmit, G.; Depla, D.; Poelman, H.; Marin, G. B.; De Gryse, R. *J. Electron Spectrosc. Relat. Phenom.* **2004**, *135*, 167.
- (33) Demeter, M.; Neumann, M.; Reichelt, W. *Surf. Sci.* **2000**, *454*, 41.
- (34) Eberhardt, M. A.; Proctor, A.; Houalla, M.; Hercules, D. M. *J. Catal.* **1996**, *160*, 27.
- (35) Thiel, P. A.; Madey, T. E. *Surf. Sci. Rep.* **1987**, *7*, 211.
- (36) Abu Haija, M.; Guimond, S.; Uhl, A.; Kuhlenbeck, H.; Freund, H. J. *Surf. Sci.* **2006**, *600*, 1040.
- (37) Okasinski, J. S.; Kim, C.-Y.; Walko, D. A.; Bedzyk, M. J. *Phys. Rev. B* **2004**, *69*, 041401.
- (38) Eng, P. J.; Trainor, T. P.; Brown, G. E.; Waychunas, G. A.; Newville, M.; Sutton, S. R.; Rivers, M. L. *Science* **2000**, *288*, 1029.
- (39) Kroger, E. A.; Allegretti, F.; Knight, M. J.; Polcik, M.; Sayago, D. I.; Woodruff, D. P.; Dhanak, V. R. *Surf. Sci.* **2006**, *600*, 4813.
- (40) Dernier, P. D.; Marezio, M. *Phys. Rev. B* **1970**, *2*, 3771.
- (41) Jin, J.; Ma, X.; Kim, C.-Y.; Ellis, D. E.; Bedzyk, M. J. *Surf. Sci.* **2007**, *601*, 3082.
- (42) Jin, J.; Ma, X.; Kim, C. Y.; Ellis, D. E.; Bedzyk, M. J. *Surf. Sci.* **2007**, *601*, 4571.
- (43) Lemire, C.; Bertarione, S.; Zecchina, A.; Scarano, D.; Chaka, A.; Shaikhutdinov, S.; Freund, H. J. *Phys. Rev. Lett.* **2005**, *94*, 166101.
- (44) Dupuis, A. C.; Abu Haija, M.; Richter, B.; Kuhlenbeck, H.; Freund, H. J. *Surf. Sci.* **2003**, *539*, 99.
- (45) Kung, H. H. *Transition Metal Oxides: Surface Chemistry and Catalysis*; Elsevier: Amsterdam, The Netherlands, 1989.
- (46) Henrich, V. E.; Cox, P. A. *The Surface Science of Metal Oxides*; Cambridge University Press: New York, 1994.
- (47) Joseph, Y.; Wuhn, M.; Niklewski, A.; Ranke, W.; Weiss, W.; Woll, C.; Schlögl, R. *Phys. Chem. Chem. Phys.* **2000**, *2*, 5314.
- (48) Bezouhanova, C. P.; Alzihari, M. A. *Catal. Lett.* **1991**, *11*, 245.
- (49) Ferretto, L.; Glisenti, A. *J. Mol. Catal. A: Chem.* **2002**, *187*, 119.
- (50) AlShihry, S. S.; Halawy, S. A. *J. Mol. Catal. A: Chem.* **1996**, *113*, 479.
- (51) Weiss, W.; Ranke, W. *Prog. Surf. Sci.* **2002**, *70*, 1.